Proceedings of ASME Turbo Expo 2014: Turbine Technical Conference and Exposition
GT2014
June 16 – 20, 2014, Düsseldorf, Germany

GT2014-27006

EFFECTS OF UNSTEADY WAKES ON FLOW THROUGH HIGH PRESSURE TURBINE PASSAGES WITH AND WITHOUT TIP GAPS

Ralph J. Volino, Christopher D. Galvin, and Cody J. Brownell
Mechanical Engineering Department
United States Naval Academy
Annapolis, Maryland 21402-5042
volino@usna.edu

ABSTRACT

Experiments were conducted in a linear high pressure turbine cascade with wakes generated by moving upstream rods. The cascade included an adjustable top endwall that could be raised and lowered above the airfoils to change the tip gap. Conditions were considered with no tip gap, and gaps of 1.5% and 3.8% of axial chord. For each of these, cases were documented both with and without upstream wakes. The pressure distributions on the airfoils were acquired at the midspan and near the tip for each case. The total pressure loss was measured in the endwall region. Velocity fields were acquired in two planes normal to the flow direction using particle image velocimetry (PIV). For the case with no tip gap, the passage vortex and other vortices were clearly visible in the velocity fields. For the cases with a tip gap, the tip leakage vortex was the dominant flow feature, and it became stronger as the gap size increased. The other vortices were still present, but were moved by the tip leakage vortex. For the cases with unsteady wakes, the PIV data were ensemble-averaged based on phase within the wake passing cycle, to show the motion and change in strength of the vortices in response to the wake passing. The regions of high total pressure loss can be explained in terms of the secondary velocity field.

NOMENCLATURE

Cp	$(P_T-P)/(\rho U_i^2/2)$, pressure coefficient
C_x	axial chord length
f	frequency
H	shape factor, displacement thickness/momentum thickness
L_s	suction surface length
P	pressure
P_T	upstream stagnation pressure
P_{Te}	downstream stagnation pressure
Re	$U_i C_x/\nu$, inlet Reynolds number
Re_θ	$U_\infty\theta/\nu$, momentum thickness Reynolds number
T	period of wake passing cycle
t	time
U_i	inlet freestream velocity
U_{rod}	wake generator velocity
U_x	axial freestream velocity
v'	rms fluctuating pitchwise velocity
w'	rms fluctuating spanwise velocity
x	axial coordinate
x_n	local streamwise coordinate
y	pitchwise coordinate
y_n	coordinate normal to local streamwise direction and to spanwise direction, distance from suction surface
z	spanwise coordinate, distance from the endwall
$\delta_{99.5}$	boundary layer thickness
ζ	U_x/U_{rod}, flow coefficient
λ	swirl strength
θ	momentum thickness
ν	kinematic viscosity
ρ	density
ψ	$(P_T-P_{Te})/(\rho U_i^2/2)$, total pressure loss coefficient

INTRODUCTION

The flow in the endwall region of a turbine airfoil passage contains a complex system of vortices. Langston [1] describes how the endwall boundary layer wraps around the leading edges of airfoils in a blade or vane row, resulting in horseshoe vortices. The turning of the flow through the passage results in the formation of the passage vortex. The pressure side leg of the horseshoe vortex merges with the passage vortex, and after crossing the passage impinges on the suction side airfoil. Others, such as Wang *et al*. [2] have identified additional vortices.

In both turbines and compressors, endwall flows contribute to aerodynamic losses, commonly referred to as secondary losses. Note that "secondary" here does not refer to the magnitude of the loss, but to the loss resulting from secondary flow. The kinetic energy contained in the vortices is unavailable to produce useful work. The secondary losses combine with the profile loss from the airfoil surface boundary layers to give the total loss for a passage. The secondary loss can be a large fraction of the total loss, particularly for low aspect ratio airfoils where the endwall regions may occupy most of the blade span. Sharma and Butler [3] note that 30 to 50% of aerodynamic losses can be due to endwall flows.

Both the hub and tip endwalls include the flow structures described above. For unshrouded airfoils, the tip endwall flow is further complicated by leakage through the gap between the airfoil tip and the

casing. The pressure difference between the two sides of an airfoil drives a flow around the tip from the pressure side to the suction side. The leakage flow reduces loading near the tip and changes the mass flow distribution around the airfoil, as indicated by Denton [4], who provides a review of all loss mechanisms. Sjolander and Amrud [5] and Xiao *et al*. [6] provide detailed measurement of the tip leakage flow structure and its effect on the blade loading near the tip. When the leakage flow exits the tip gap and moves into the endwall boundary layer on the suction side of the passage, the resulting shear causes the flow to roll up into the tip gap vortex, which can then interact with the other vortices in the endwall region. Harvey [7] showed that a vortex generated from the tip leakage flow will persist and continue to induce losses in subsequent turbine blade rows. It is therefore important to reduce the strength of this vortex if possible. Booth [8] indicated that tip leakage flow can account for 1/3 of total losses. Payne *et al*. [9] conducted experiments and computations to obtain the unsteady entropy at one vane position at the exit from a high pressure turbine stage. They showed that there were four major loss mechanisms: (1) the tip leakage vortex, (2) the upper passage vortex, (3) the wake vortex, and (4) the lower passage vortex. Of these the largest source of rotor loss was clearly the tip leakage vortex, which extended down to approximately 75% height and across nearly 75% of the blade pitch in their study. The magnitude of the tip gap loss depends on the gap size. As noted in Behr [10], reducing the tip gap size by as little as 0.25 mm could lead to as much as a 1% reduction in fuel consumption, but as indicated by Lattime and Steinetz [11], the change in tip gap size during operation of a typical large engine is over three times this amount, so simply reducing the tip gap may not be possible.

Many studies have considered endwall boundary layers under steady flow conditions in turbine cascades. Documentation has included total pressure loss, time-averaged mean velocity and turbulence fields, and heat transfer on both the endwall and airfoil surfaces. Some examples include Gregory-Smith and Cleak [12], and MacIsaac *et al*. [13]. Wang *et al*. [14] provide velocity field measurements acquired with particle image velocimetry (PIV) in a tip leakage study. These studies clearly show the losses associated with the endwall vortices and their location within passages. These examples are a small subset of the available literature, as secondary flows have been extensively studied.

Steady flow cascade studies miss the important effect of periodic unsteadiness in engines. Vanes and rotor blades move relative to each other, causing downstream airfoils to move through the wakes shed by the blade and vane rows upstream. Behr [10] provides a description of the interaction between airfoil rows. The wakes include a velocity deficit and elevated turbulence as described by Hodson and Howell [15]. The "negative jet" associated with the velocity deficit and the turbulence can have a strong influence on the boundary layers on both the airfoils and the endwalls. The situation is further complicated at the endwall, as vortices generated in one passage persist and periodically interact with vortices generated in downstream passages. Behr [10] lists several studies which have considered this effect, including Chaluvadi *et al*. [16], and Boletis and Sieverding [17].

To document the effect of periodic wakes, some studies have utilized cascades with moving upstream bars, while others have used rotating facilities, some with multiple stages. Documentation in unsteady flows often includes time-averaged total pressure and heat transfer results. In some cases instantaneous results are also provided to show the transient effect of the wake passing. Examples include Prasad and Wagner [18] and Behr [10] who obtained unsteady pressure results. In the case of Behr [10] these pressure results were obtained with a traversing probe in the flow and provide quite detailed information about the instantaneous flow structure. These studies are the exception, however, and documentation of instantaneous flow fields is limited. Behr [10] indicated that future work should include more time resolved velocity field measurements.

Tip leakage flow, with or without the presence of upstream wakes, is influenced by the motion of the rotor blades relative to the turbine casing, which results in a shearing of the flow in the tip gap. The shear acts in opposition to the pressure force driving the leakage flow. The relative motion also tends to move the tip gap vortex closer to the suction side of the passage. The importance of the endwall motion depends on the size of the tip gap. Palafox *et al*. [19] found that endwall motion was important in cases with the tip gap size ranging up to 3% of blade chord. Srinivasan and Goldstein [20] reported a small effect of wall motion for a tip gap of 0.6% of chord. For larger tip gaps the flow was pressure driven and the relative motion had little effect. Krishnababu *et al*. [21] considered tip gaps of 1.6% and 2.8% of chord and found the effects of relative motion to be small. They concluded that it may not be worth the effort to include the moving wall in experiments depending on the focus of the study.

The present work is a continuation of a study that addresses the need for documentation of secondary flow fields during wake passing events. Periodic wakes were produced by moving rods upstream of a linear cascade. The eventual goal is to document experimentally and to predict computationally the instantaneous velocity field in the endwall region in cases with and without tip gaps, to relate these fields to secondary losses, and to test methods for controlling the secondary flows to reduce losses. Earlier work, presented in Volino *et al*. [22], documented loading on the blades and time-averaged total pressure loss fields in the endwall region for cases without a tip gap. Also presented was the inlet flow field to the cascade both at the midspan and in the endwall boundary layer. Instantaneous results were included for cases with upstream wakes as well as comparison cases with steady inflow (no wakes). Velocity data at the exit of the cascade were presented at the midspan for cases with and without wakes. The present paper extends the results for the case with no tip gap and also includes new cases with two different tip gaps. Documentation includes total pressure loss in the endwall region and instantaneous velocity fields in the passage acquired with PIV.

EXPERIMENTAL FACILITY AND MEASUREMENTS

Experiments were conducted in a closed loop wind tunnel with a seven blade linear cascade in one corner of the loop, as shown in Fig. 1. A tailboard was positioned to produce periodicity. The airfoils were two dimensional and the shape was the General Electric E^3 (Energy Efficient Engine), high pressure turbine, stage 1 rotor blade tip cross section [23,24]. Details are provided in Table 1. The inlet flow angle was 38.8°. The exit metal angle was 60°, and the design exit flow angle was 64.4°. The actual average exit flow angle, determined with PIV measurements, was 61.5°. The blade spacing was equal to the axial chord, C_x. The cascade blades had a high aspect ratio (span/C_x) of 4.8. This aspect ratio was much higher than in the E^3 design, which had a span approximately equal to C_x. The large span was chosen to simplify the flow by ensuring that the boundary layers on the two endwalls would not merge. Since the span in the experiments was not representative of engine conditions, C_x is used below as the normalizing quantity for the tip gap size. The top endwall was a false ceiling in the tunnel and was moved up and down to produce different tip gaps above the cascade blades. The false ceiling was divided into two pieces with one piece above the blades, and the other upstream. A gap of about $0.1C_x$ was needed between the pieces of the endwall for the rods in the wake generator (described below) to pass. The gap also served as a suction slot and bled off part

of the endwall boundary layer before it reached the blades. Conditions of the endwall boundary layer downstream of this slot, for the case without rod wakes, are presented in Table 2, with further details available in Volino *et al*. [22].

A coarse grid located upstream of the cascade was used to break up the boundary layers which formed upstream of the test section, providing uniform inlet conditions to the cascade and elevated freestream turbulence. In a plane parallel to the cascade, $1.7C_x$ upstream of the leading edges, the grid produced a mean flow that was uniform outside the endwall boundary layer to within ±3%. The streamwise component of the freestream turbulence in this plane was 5%, and the cross stream component was 4.5%. The freestream turbulence was also measured at the inlet plane of the cascade in passage 3-4 (between blades B3 and B4) and passage 4-5. The streamwise component intensity was 4% in both passages and the cross stream component intensity was 3.6%. At the exit plane of the blade row, the streamwise component intensity was 1.5%. The change through the passage was due mainly to the change in the local freestream velocity along with some decay of the turbulence. If normalized on the inlet velocity, the exit intensity would be 2.6% in the streamwise component and 3.2% in the cross stream component. The upstream integral length scale of the freestream turbulence was $0.15C_x$ in the streamwise component and $0.04C_x$ in the cross stream component.

The wake generator included a chain near each endwall that passed $0.58C_x$ upstream of the leading edges of the cascade blades. The chains then passed downstream around blade B1 on the inside turn of the cascade and passed well downstream of the cascade before returning upstream around blade B7 on the outside turn of the cascade. The magenta line surrounding the cascade in Fig. 1 shows the location of the chain. The chain links had hollow pins, through which the wake generator rods were attached. Each rod was a 4 mm diameter carbon fiber tube with a steel pin attached at each end. The steel pins were inserted through the holes in the upper and lower chain. The distance between rods was $0.96C_x$, which corresponded as closely as possible to the blade spacing, given that an integer number of chain links was required. The upstream vane spacing was 1.6 times the blade spacing in the E^3 design. A ratio of 1 was chosen in the present study to allow flow in a single blade passage to be calculated with periodic boundary conditions in future computational work.

The rods were driven at a velocity equal to the cascade axial velocity, U_x, to produce a flow coefficient, $\zeta = U_x/U_{rod} = 1.0$. The wake passing frequency was 21 Hz, corresponding to a dimensionless frequency $fC_x/U_x = 1.05$ which was approximately equal to the value for the E^3 design. The timing of the wake generator was recorded with an infrared photo detector, which sensed the passage of each rod and emitted a voltage that was used to trigger the acquisition of PIV images.

The ratio of the rod diameter to the axial chord was 0.03. This equaled the ratio of the trailing edge diameter of the E^3 stage 1 vane to the blade axial chord. The velocity deficit and turbulence level in the rod wakes were a good approximation to a blade wake, as documented in Volino *et al*. [22]. At the cascade inlet, the peak turbulence intensity in the rod wakes was 14%, and the level between wakes matched the background turbulence intensity (4%) in the wind tunnel.

Data were acquired at Re=30,000 based on the inlet velocity and axial chord. The Mach number was 0.01. The Reynolds number was very low compared to engine conditions, but was limited by the facility, in particular the speeds achievable by the wake generator while maintaining a representative flow coefficient. The study still captured many of the important effects of endwall and tip leakage flows, however, including the important vortices. Cases were documented with no tip gap, a small tip gap of 1.5% of C_x, and a large gap of 3.8% of C_x.

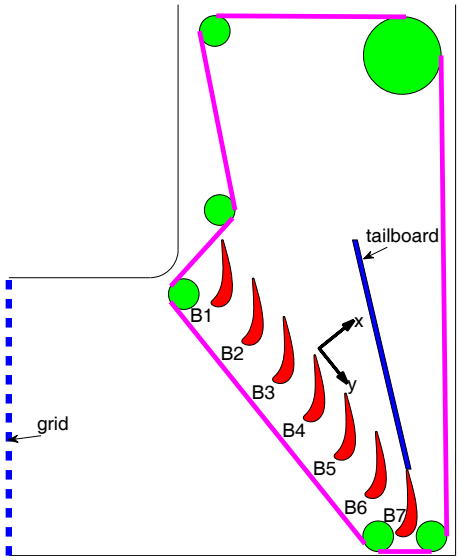

Fig. 1 Schematic of linear cascade with wake generator.

Table 1: Cascade parameters.

Axial Chord, C_x [mm]	True Chord [mm]	Pitch [mm]	Span [mm]	Suction side, L_s [mm]	Inlet flow angle	Des.exit flow angle
132.6	163	132.6	635	230	38.8°	64.4°

Table 2: Inlet endwall boundary layer parameters.

$\delta_{99.5}/C_x$	θ/C_x	Re_θ	H
0.457	0.020	614	1.22

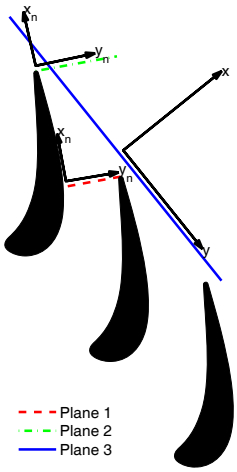

Fig. 2 Measurement planes for PIV and total pressure.

Measurements

The center blade, designated B4 in Fig. 1, contained pressure taps near the spanwise centerline and $0.1C_x$ from the tip. Blades B3 and B5 contained pressure taps on their suction and pressure sides respectively, at the same spanwise locations. Hence the pressure distributions were documented for passages 3-4 and 4-5. Pressure surveys were made using a pressure transducer (0-500 Pa range

Validyne transducer). Pressure transducer readings were acquired at a 10 kHz sampling rate over a 10 second period and averaged. Stagnation pressure was measured with a pitot tube upstream of the cascade and wake generator. The pressure coefficient, *Cp*, was computed as the difference between the upstream total pressure and the local static pressure normalized on the upstream dynamic pressure. The uncertainty in *Cp* was 6%. Results in Volino *et al*. [22] showed that *Cp* in the two passages agreed to within about 8%. Data acquired subsequent to those in the present paper (see Volino [25]) showed that better adjustment* of the cascade resulted in agreement between the passages within 3%, and the new data agreed very well with the passage 3-4 data of the present paper. Only the passage 3-4 data, therefore, are presented below.

Total pressure losses were documented using a Kiel probe traversed $0.1C_x$ downstream of the cascade. A traverse was located in the wind tunnel downstream of the cascade to move the probe. The flow blockage caused by the traverse was checked [26] and found to be acceptably low when it was located at least $2C_x$ downstream of the cascade. Variations in the wind tunnel velocity were less than 2% as the traverse was moved to various positions. The probe was traversed through a grid across 2.2 blade spacings and extending from 0 to $0.87C_x$ from the endwall (plane 3 in Fig. 2). The grid spacing in both directions was $0.038C_x$. The uncertainty in the loss coefficient, ψ, was 6%.

Velocity fields were measured using PIV. Image pairs were acquired using a 250 mJ, 8 ns pulse YAG laser (*Quantel CFR 400*) and 4 megapixel camera (*TSI PowerView Plus* with *Nikkor* micro 55 mm lens). The typical time delay between the images in each pair was between 55 and 100 μs. The flow was seeded with olive oil particles using an atomizer (*TSI 930706*). For all cases and image planes considered, 1000 image pairs were acquired. For cases with upstream wakes, the laser firing was triggered based on the wake passing. For these cases, images were taken as 10 sets of 100 pairs, with each set at a specific time delay after the passing of a wake. The 10 different delays were evenly spaced within the wake passing period. Velocity vectors were computed from the images using *TSI Insight 3G* software with a recursive grid (64×64 pixels with 50% overlap in both passes).

Data were acquired in the planes shown in Fig. 2. The laser sheet entered through the top endwall and the camera was located inside the wind tunnel, downstream of the cascade. Plane 1 was located normal to the main flow in passage 3-4 with one side at the trailing edge of the pressure side blade. Plane 2 was located farther downstream in the same passage, normal to the main flow, with one side at the trailing edge of the suction side blade.

RESULTS

Cp Distribution

The static pressure on the airfoils is shown for all cases in Fig. 3. At the midspan (Fig. 3a), all cases agreed with each other. Upstream wakes did not change the loading for these cases. The midspan location was too far from the endwall for the results to be affected by the tip gap. At the location $0.1C_x$ from the tip (Fig. 3b), the wakes still had no significant effect, but there was a change in loading with different tip gaps. The endwall boundary layer resulted in reduced loading (lower suction side *Cp*) for all cases compared to the midspan

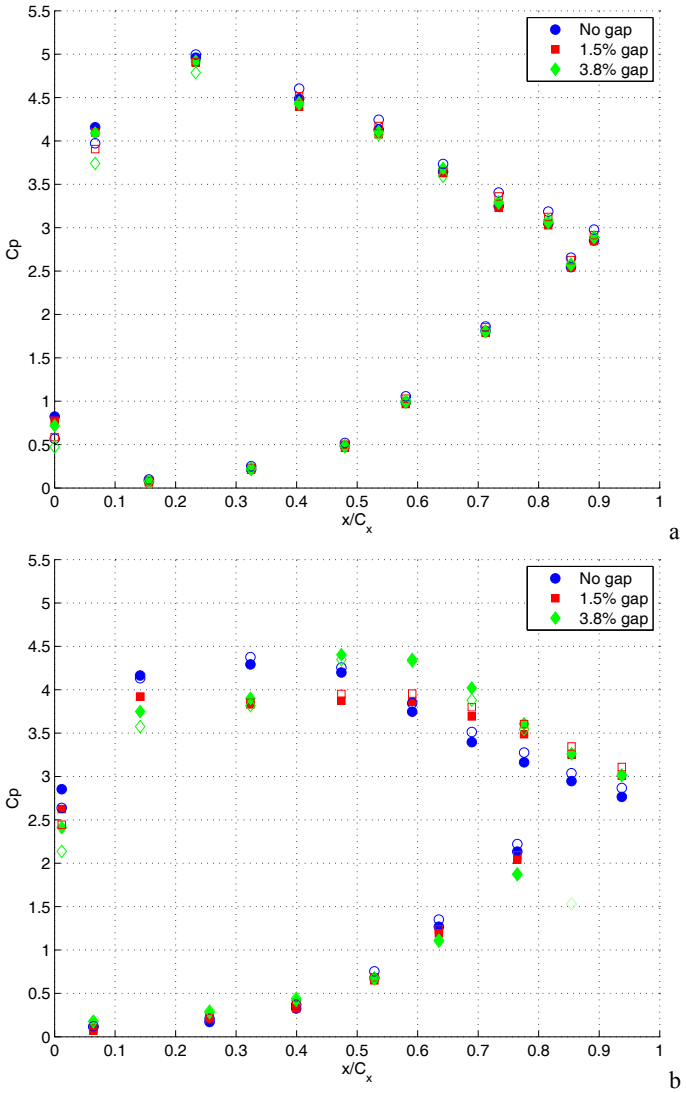

Fig. 3 *Cp* profiles, solid symbols – without wakes; open symbols – with wakes: a) midspan, b) 0.1 C_x from tip.

results. Increasing the tip gap size moved the suction peak downstream, reduced the suction side *Cp* on the upstream part of the blade, and increased *Cp* near the trailing edge.

Velocity and Total Pressure Loss

No tip gap, no wakes. Typical instantaneous and the time-averaged velocity fields for planes 1 and 2 are shown in Fig. 4 for the case with no tip gap or wakes. Contours of the swirl strength corresponding to the velocity vectors are also shown in each plot. The swirl strength, λ, can be used to locate vortices. It is closely related to the vorticity, but discriminates between vorticity due only to shear and vorticity resulting from rotation. It is defined as the imaginary part of the complex eigenvalue of the local velocity gradient tensor, and was used in the present study in a two-dimensional form as explained in Hutchins *et al*. [27]. By definition, λ is always ≥0, but a sign can be assigned based on the local vorticity to show the direction of rotation. Positive swirl indicates counterclockwise rotation in the view of the figures in this paper, which are looking downstream through the cascade. The suction side of the passage corresponds to y_n/C_x=0, and

* It was discovered that one of the blades (which were cantilevered from the bottom endwall) was inclined at about 0.2 degrees from vertical. While too small an inclination to see, it did make a small difference in the pressure distribution, particularly for passage 4-5.

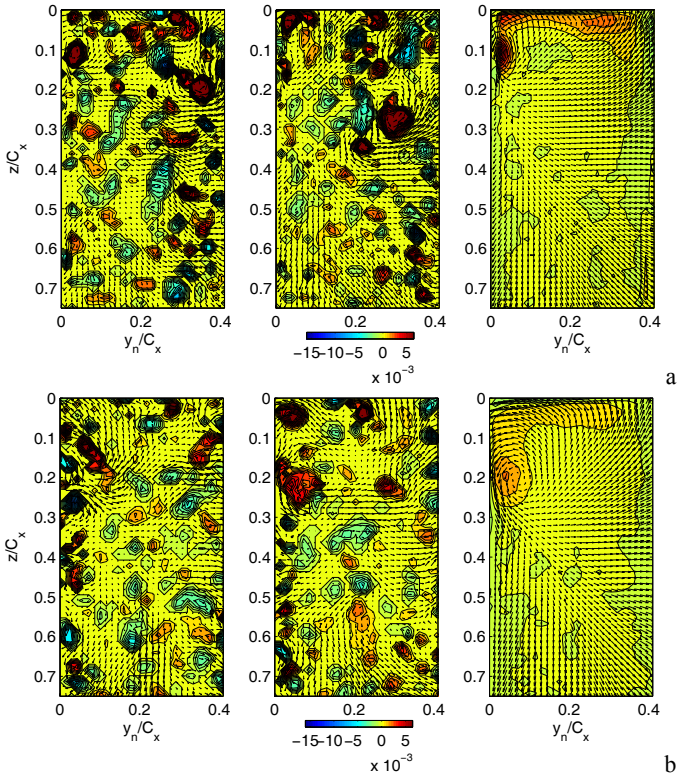

Fig. 4 Vector fields and swirl strength ($\lambda C_x/U_i$). No tip gap, no wakes. Columns 1 & 2 – typical instantaneous. Column 3 – time-averaged: a) plane 1, b) plane 2.

the pressure side is located at $y_n/C_x \approx 0.4$. On the vertical axis, $z/C_x=0$ is at the top endwall. The instantaneous flow fields showed many vortices of both clockwise and counterclockwise rotation throughout the field of view. The pattern of the vortices appeared random, as one might expect for a turbulent flow. Significant vorticity existed outside the endwall and blade boundary layers, which may be attributed to the elevated freestream turbulence and/or to structures originating in the boundary layers that occasionally extended farther from the walls. No particular vortex stood out in the instantaneous fields. In the time-averaged field, however, three distinct vortices were clear, and all had positive swirl. There was a region of positive swirl near the endwall with a vortex in the corner at the junction of the suction surface and the endwall and another vortex at $y_n/C_x \approx 0.25$. The vortex at the endwall-suction surface junction may be the corner vortex, shown in studies such as Wang *et al.* [2]. The corner vortex is induced by the suction side leg of the horseshoe vortex. The corner vortex is typically weak, however, and the suction side leg of the horseshoe vortex (which would have negative swirl) was not visible, so it is not entirely clear if the region of positive swirl in the upper left corner of Fig. 4 is the corner vortex. The strongest vortex in Fig. 4 was located along the suction surface at $z/C_x=0.1$ in plane 1 and $z/C_x=0.2$ in plane 2. This was clearly the passage vortex, which had crossed the endwall and was moving along the suction surface away from the endwall. The overall strength of this vortex was about the same in planes 1 and 2, but it had grown and spread over a larger area at the downstream plane. This change in size may have been due to an actual increase of the average instantaneous size of the vortex, but it may also indicate that the vortex was moving more at plane 2, so that in a time-averaged sense it appeared spread over a larger area.

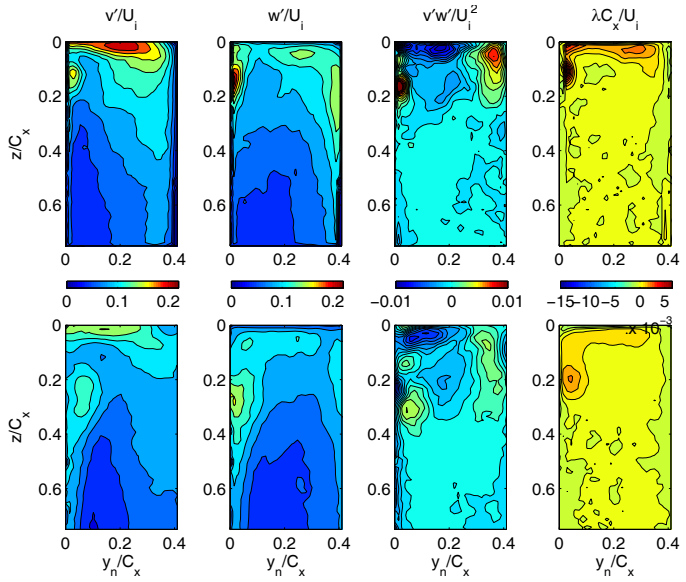

Fig. 5 Time-averaged turbulence quantities and swirl in planes 1 (top) and 2 (bottom). No tip gap, no wakes.

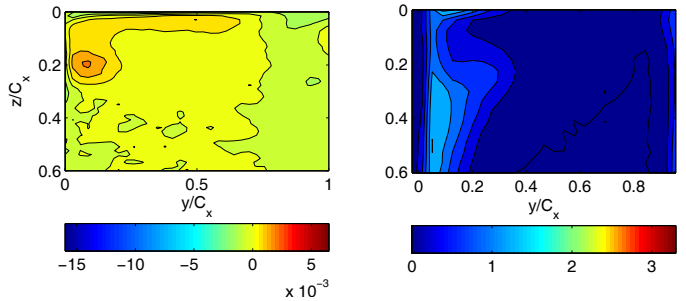

Fig. 6 Time-averaged $\lambda C_x/U_i$ (left) and ψ (right). No tip gap, no wakes.

Figure 5 shows the rms turbulence quantities, v' and w' corresponding to the horizontal (pitchwise) and vertical (spanwise) components of the turbulence in planes 1 and 2. Also shown are the time-averaged Reynolds shear, $v'w'$, and swirl strength. The turbulence was high in the endwall boundary layer and around the passage vortex. The areas of high magnitude $v'w'$ corresponded to regions of high average shear induced by the secondary flow.

Figure 6 compares the time-averaged swirl strength in plane 2 to the total pressure loss coefficient in plane 3. To facilitate the comparison, the horizontal axis for the swirl strength was projected from plane 2 onto plane 3 by dividing the plane 2 y_n location by the cosine of the exit flow angle. Direct measurement of the velocity field in plane 3 for a few cases showed that although plane 3 contained a component of the streamwise velocity, the swirl strength fields in planes 2 and 3 were very similar. The highest loss occurred in the wake of the airfoil near $y/C_x=0$. There was also a bulge of high loss near $z/C_x=0.2$ that extended farther into the passage. This loss was associated with the passage vortex. Some loss may have been generated by the turbulence and shear caused by the vortex. The vortex also entrained fluid with high loss from the suction surface boundary layer and moved it out into the passage, and fluid from the freestream was moved toward the suction surface at $z/C_x=0.1$, causing lower loss at this location.

No tip gap, with wakes. The addition of wakes did not greatly change the time-averaged flow structure, but some effects of the wakes

were detectable. Figure 7 shows the pitchwise component of the pitchwise-averaged, ensemble-averaged freestream turbulence at z/C_x≈0.8, which was far enough from the endwall to match the behavior at midspan. The spanwise component of the turbulence (not shown) behaved similarly. In plane 1, at the phases t/T=0.1 to 0.4, the turbulence was low, corresponding to the period between rod wakes. At t/T=0.5 the turbulence began to rise as the rod wake appeared, and then remained high for t/T=0.6 to 0.8, before falling at t/T=0.9. In plane 2, the rod wake appeared at t/T=0.9, persisted until t/T=0.3, and the period between wakes occurred from t/T=0.4 to 0.8. The appearance of the wake was delayed by half a cycle between planes 1 and 2, which matched the time needed for the flow to convect from plane 1 to 2. Rod wake data acquired upstream of the cascade and presented in Volino *et al*. [22] showed that the wakes spread as they moved through the passage and occupied a larger fraction of the cycle at the downstream locations.

Phase-averaged swirl strength is shown in Fig. 8 using the same coordinates and color scale used in Figs. 4-6. The appearance of the rod wake caused the passage vortex to move closer to the endwall. In plane 1 at t/T=0.2 to 0.5 the center of the passage vortex was at about z/C_x=0.13. This corresponded to the time between wakes, and the vortex location agreed with the location for the case without wakes shown in Fig. 5. The wake effect appeared strongest at t/T=0.8 and 0.9, and the center of the vortex moved to about z/C_x=0.08. Comparison to Fig. 7a indicates that there was a phase lag of about 0.1T between the appearance of the wake in the turbulence and the response of the passage vortex. The behavior in plane 2 was similar, with the passage vortex located at roughly z/C_x=0.2 at t/T=0.5 to 0.9 in the period between wakes, and moving toward about z/C_x=0.14 at t/T=0.1 to 0.4 in response to the wake. The location between wakes was about the same as in the case without wakes shown in Fig. 5. Comparison to Fig. 7b again shows a phase lag of about 0.1T between the rod wake turbulence and the response of the vortex.

Figure 9 shows the swirl strength of Fig. 8 averaged across the blade pitch from y_n/C_x=0 to 0.4 and plotted as a function of distance from the endwall. There was a peak at all phases at z/C_x=0.03 in plane 1 and z/C_x=0.05 in plane 2 corresponding to the vorticity in the endwall boundary layer. There was a second peak between z/C_x=0.1 and 0.15 in plane 1 and between z/C_x=0.15 and 0.25 in plane 2 corresponding to the passage vortex. The second peaks were largest during the phases between wakes, and lower during the wakes as the passage vortex moved toward the endwall.

The time-averaged swirl and total pressure loss are compared in Fig. 10 using the same format and color range as in Fig. 6. Comparing the swirl in Figs. 6 and 10, the two cases were very similar, but the time-averaged center of the passage vortex was slightly closer to the endwall in the case with wakes (Fig. 10), due to the effect of the wakes during part of the cycle shown in Fig. 8. The total pressure loss was similar in the cases with and without wakes, but was slightly higher with the wakes due to the losses associated with the rod wakes themselves, and the effect of the rod wake turbulence in increasing the losses in the boundary layers. The loss is quantified below and was also discussed in Volino *et al*. [22] for the cases without a tip gap.

1.5% tip gap, without wakes. Sample instantaneous velocity vector and swirl fields along with the time-averaged fields for planes 1 and 2 are shown in Fig. 11 for the case with 1.5% C_x tip gap. As in Fig. 4 for the case with no tip gap, the instantaneous fields showed a random appearing assortment of clockwise and counterclockwise vortices. Inspection of many instantaneous fields, however, showed a preponderance for negative swirl near the endwall, and this appeared clearly in the time-averaged field near the endwall – suction surface

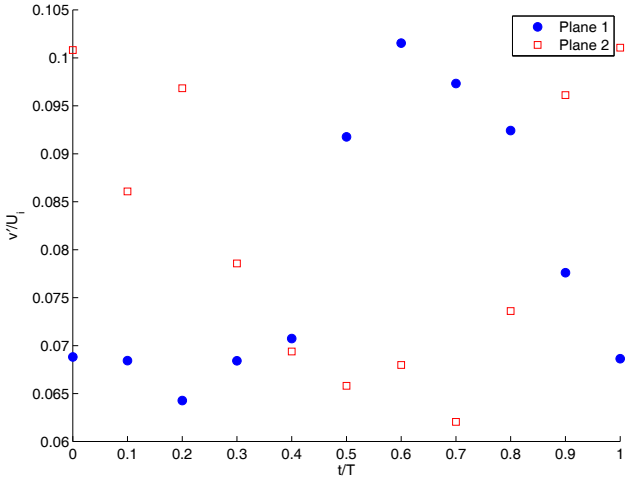

Fig. 7 Phase-averaged turbulence at midspan, no tip gap.

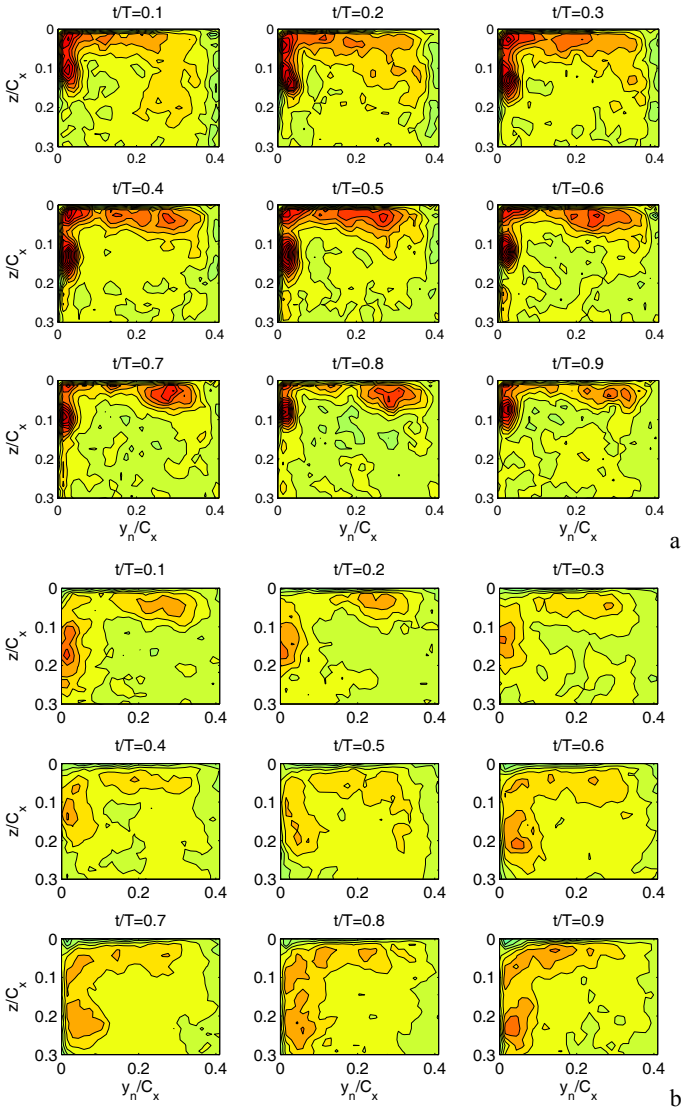

Fig. 8 Phase-averaged swirl, no tip gap: a) plane 1, b) plane 2.

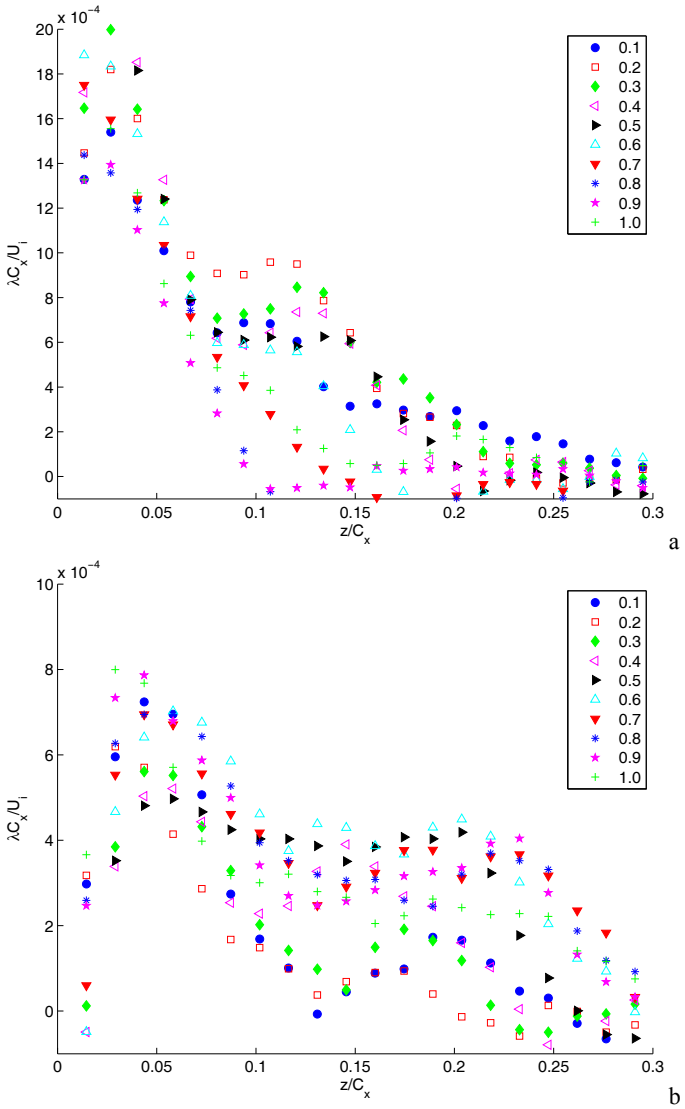

Fig. 9 Phase-averaged and pitchwise averaged swirl: a) plane 1, b) plane 2. No tip gap. Legend indicates wake passing phase from *t/T*=0.1 to 1.

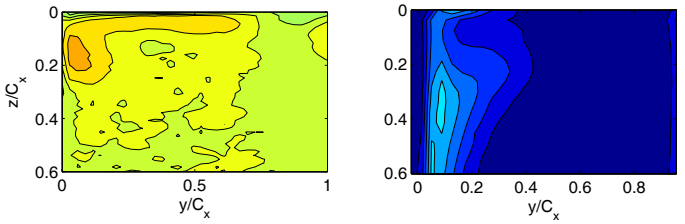

Fig. 10 Time-averaged $\lambda C_x/U_i$ (left) and ψ (right). No tip gap, with wakes.

corner in both planes 1 and 2. This was the tip leakage vortex. It was much stronger than the other vortices, with a maximum swirl strength about three times larger and opposite in sign to the maximum swirl in the passage vortex. Between planes 1 and 2 the tip leakage vortex grew in size and penetrated farther across the passage toward the pressure side. The maximum swirl strength in the tip leakage vortex decreased between planes 1 and 2 such that the total vorticity remained

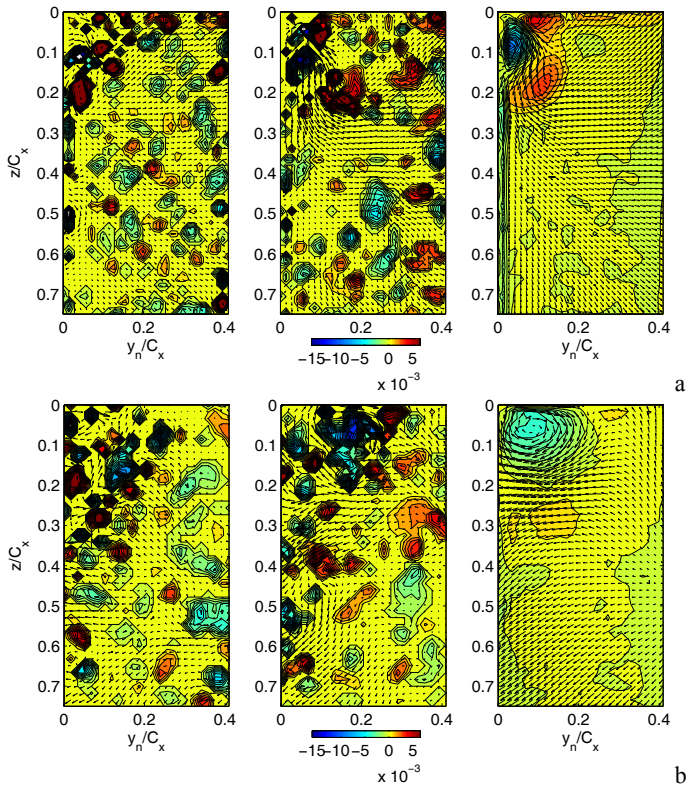

Fig. 11 Vector fields and swirl strength ($\lambda C_x/U_i$). 1.5% tip gap, no wakes. Columns 1 & 2 – typical instantaneous. Column 3 – time-averaged: a) plane 1, b) plane 2.

about the same in the two planes. As noted in Bunker [28], the maximum leakage is expected to occur where the blade loading is strongest. The loading in Fig. 3 and the measurement locations in Fig. 2 suggest that much of the leakage had occurred by plane 1, so the vortex did not grow much in strength farther downstream. The passage vortex and the counterclockwise rotating vortex near the endwall-suction surface junction seen in Fig. 4 are still clearly visible in Fig. 11, but have moved away from the suction surface in response to the tip leakage flow. The passage vortex has also moved farther from the endwall. The near wall vortex was located at y_n/C_x=0.1, z/C_x=0.02 in plane 1 and y_n/C_x=0.28, z/C_x=0.03 in plane 2. The passage vortex was located at y_n/C_x=0.11, z/C_x=0.2 in plane 1 and y_n/C_x=0.14, z/C_x=0.29 in plane 2. The clockwise rotating tip leakage vortex would also tend to induce these counterclockwise rotating vortices to be stronger.

The turbulence quantities are compared to the swirl strength in Fig. 12, in the same format as Fig. 5. The color scale for the swirl strength is the same for all figures in the paper, but the color scale for the turbulence was changed to show the much higher turbulence in cases with tip leakage flow. All the turbulence quantities were highest around the leakage vortex and were particularly high where the leakage flow exited the tip gap in plane 1. The shear layers generated by the leakage flow resulted in positive and negative regions of $v'w'$.

The swirl strength and total pressure loss are compared directly in Fig. 13. Clearly the dominant region of high loss was due to the leakage flow, and this loss was much higher than in the case with no tip gap of Fig. 6. The passage vortex was still present and extended the high loss region to y/C_x=0.2 and z/C_x=0.3.

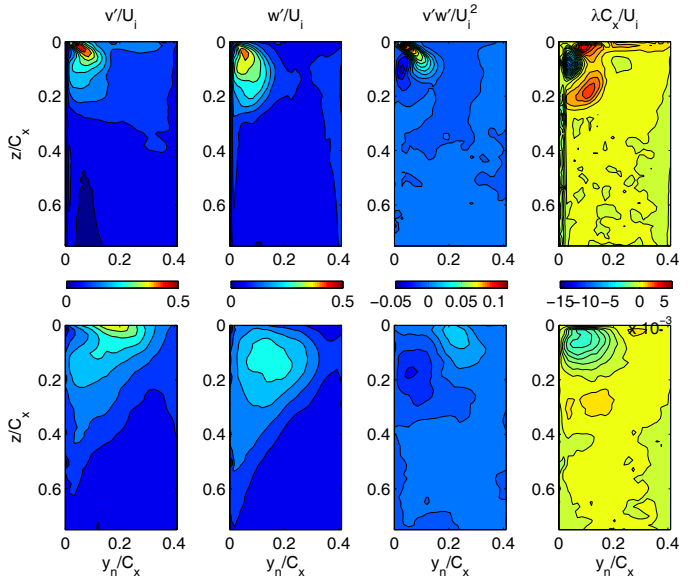

Fig. 12 Time-averaged turbulence quantities and swirl in planes 1 (top) and 2 (bottom). 1.5% tip gap, no wakes.

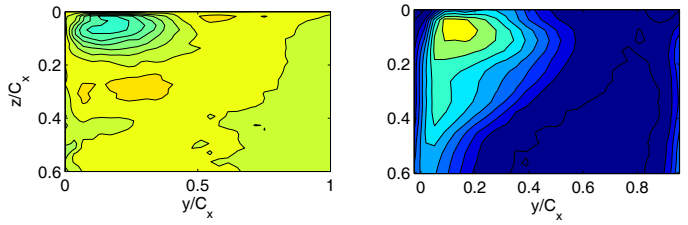

Fig. 13 Time-averaged $\lambda C_x/U_i$ (left) and ψ (right). 1.5% tip gap, no wakes.

1.5% tip gap, with wakes. The phase-averaged results for the case with 1.5% tip gap and rod wakes are shown in Figs. 14 and 15. The midspan turbulence (not shown) matched the results of Fig. 7, to within small differences in the timing of the wake of about 0.1*T*. The agreement with Fig. 7 was expected since the presence of the tip gap should have no impact on the rod wake at midspan. Fig. 14 shows the swirl strength. In plane 1, the tip leakage vortex did not change significantly with the wake. It may have been too strong and concentrated to be affected by the wake. The passage vortex, similarly, showed little response to the rod wake. There was little difference from the case without wakes of Fig. 12. In plane 2, the wake had some effect. The vortices identified in Fig. 12 were most distinct and concentrated at the phases between wakes, t/T=0.5 to 0.7, during which there was good agreement with the no-wake case results. During the wake, at t/T=0.1 to 0.3, the leakage vortex was spread over a wider area as it was influenced by the wake, and the passage vortex was no longer clearly visible. It is possible that the wake turbulence caused mixing of the fluid in the vortex with the surrounding fluid, but it is also possible that the vortex was still present but moving so that it did not appear clearly in the phase-averaged results. Figure 15 shows the pitchwise averaged swirl. The figure is similar to Fig. 9, but the positive and negative swirl regions were averaged separately. For the positive swirl average, regions where the swirl strength was negative were assigned a value of zero for the average. Similarly, for the negative swirl average, regions of positive swirl were set to zero for the average. In plane 1 (Fig. 15a), there was a negative peak

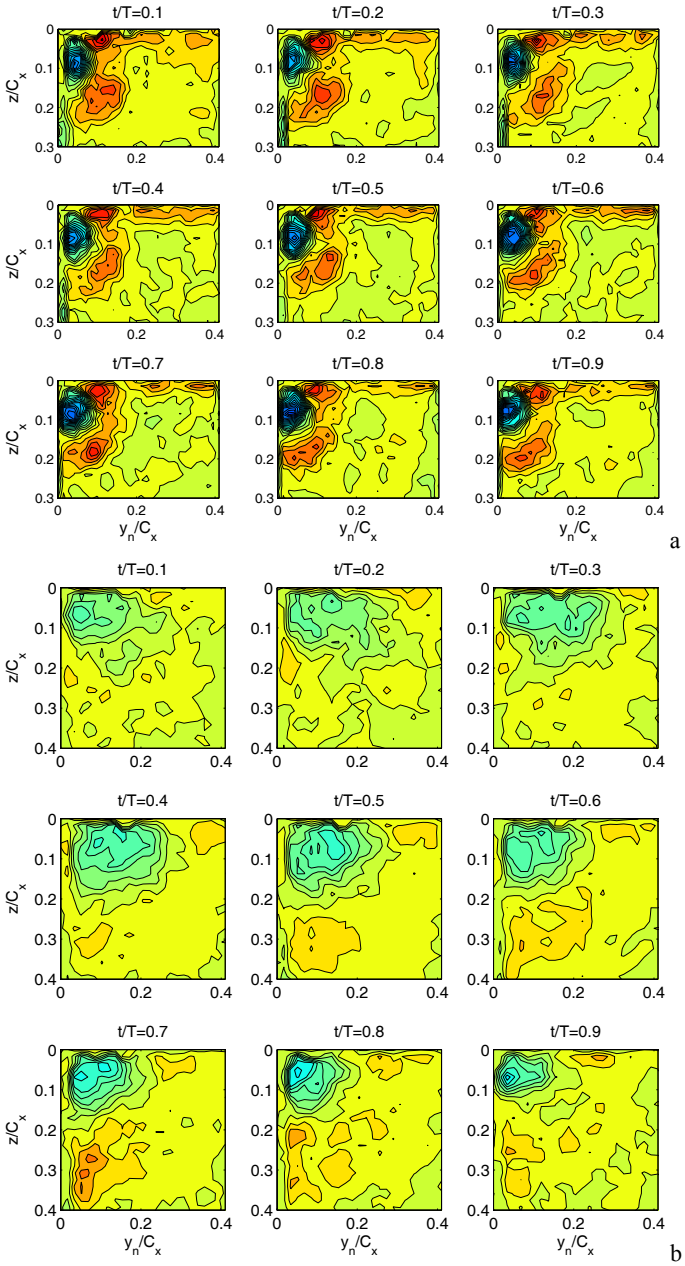

Fig. 14 Phase-averaged swirl, 1.5% tip gap: a) plane 1, b) plane 2.

associated with the leakage vortex at z/C_x=0.9 and a positive peak associated with the passage vortex at z/C_x=0.17. The results at the different phases were not much different from each other, but the negative peak was somewhat stronger at the phases within the wake. In plane 2 there was more variation, corresponding to the differences seen in Fig. 14. As in plane 1, the negative swirl was strongest within the wake. The positive peak had the opposite trend, with higher values between wakes, in agreement with the dispersal of the passage vortex seen in Fig. 14.

Figure 16 compares the swirl strength and total pressure loss. There was not much difference from the case without wakes in Fig. 13. The highest loss was clearly in the region of the leakage vortex. The losses appeared to be slightly higher overall with the wakes, but the peak was

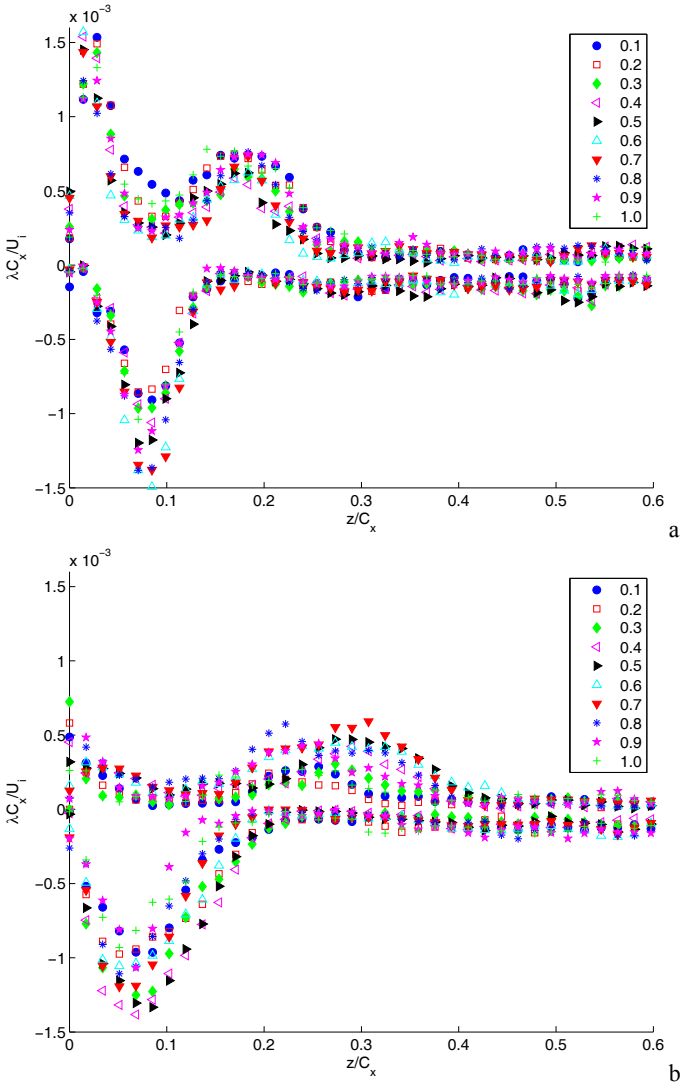

Fig. 15 Phase-averaged and pitchwise averaged swirl: a) plane 1, b) plane 2. 1.5% tip gap. Legend indicates wake passing phase from *t/T*=0.1 to 1. Phase-averaged positive and negative swirl are pitchwise averaged separately.

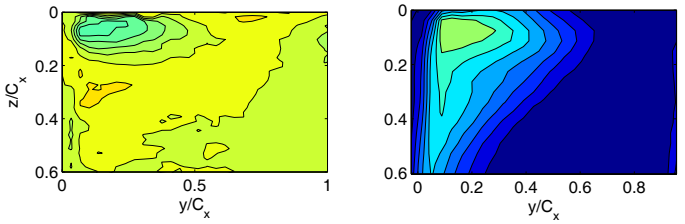

Fig. 16 Time-averaged $\lambda C_x/U_i$ (left) and ψ (right). 1.5% tip gap, with wakes.

actually higher in the case without wakes. As will be shown in spatially averaged results below, these differences were small.

3.8% tip gap, without wakes. Instantaneous and time-averaged velocity vector and swirl fields for the case with 3.8% C_x tip gap are shown in Fig. 17. In many of the instantaneous velocity fields in both planes 1 and 2, including three of the four shown in Fig. 17, there was

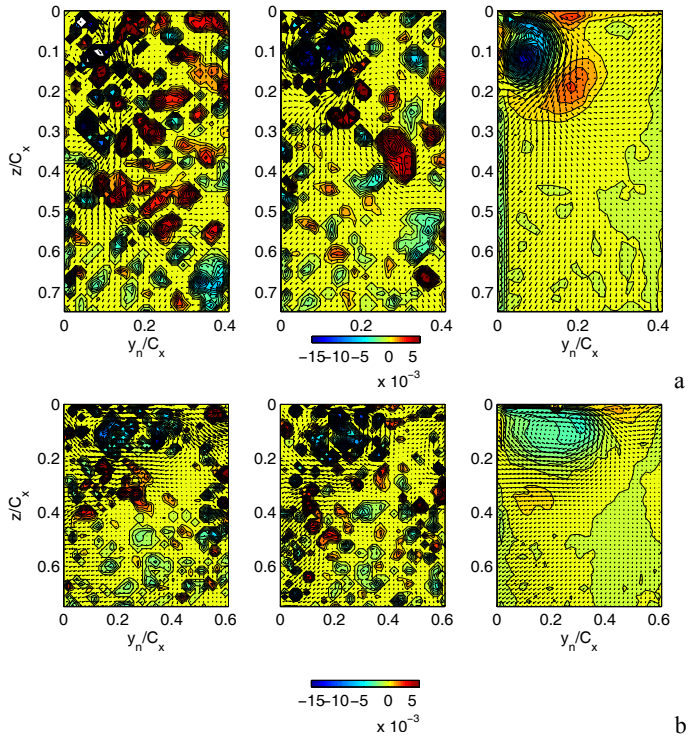

Fig. 17 Vector fields and swirl strength ($\lambda C_x/U_i$). 3.8% tip gap, no wakes. Columns 1 & 2 – typical instantaneous. Column 3 – time-averaged: a) plane 1, b) plane 2.

a concentration of negative swirl near the endwall, and this was evidenced clearly in the time-averaged fields as a very strong leakage vortex. In plane 1, a strong jet was visible leaving the tip gap at y_n/C_x=0 and z/C_x=0, and upon interacting with the main flow in the passage, this jet rolled up into the leakage vortex. As in Fig. 11, the passage vortex and the counterclockwise vortex closer to the endwall were clearly visible, but with the stronger leakage flow in Fig. 17, they have migrated farther from the endwall and farther toward the pressure side of the passage. In plane 1, the near wall vortex was located at y_n/C_x=0.18, z/C_x=0.02, and the passage vortex was located at y_n/C_x=0.18, z/C_x=0.2. For plane 2, the field of view in Fig. 17 has been expanded in the horizontal direction. This plane, as shown in Fig. 2, extended beyond the trailing edge of the blade on the pressure side of the passage. The strong leakage flow caused the vortex near the endwall to move to y_n/C_x=0.44, z/C_x=0.02, and the passage vortex was rolled under the leakage vortex to y_n/C_x=0.15, z/C_x=0.35. The pitchwise averaged results for the 3.8% tip gap cases in plane 2 were averaged from y_n/C_x=0 to 0.6 instead of to 0.4 as was done for all the other cases.

Turbulence quantities are shown with the swirl strength in Fig. 18. The turbulence was stronger than in the case with smaller tip gap, and the color range on the contour plots was expanded to accommodate this. In plane 1 the turbulence was high in and around the leakage vortex, and the shear was high and of opposite sign on opposite sides of the vortex. In plane 2, the strongest swirl was well away from the suction surface at y_n/C_x=0.3 and the highest turbulence and shear were located around it. Figure 19 compares the swirl and total pressure loss, and shows that the highest loss corresponded to the high swirl of the leakage vortex. The loss was much higher than in the case with the smaller tip gap and the region of high loss extended to the area of the passage vortex at y_n/C_x=0.2 and z/C_x=0.35.

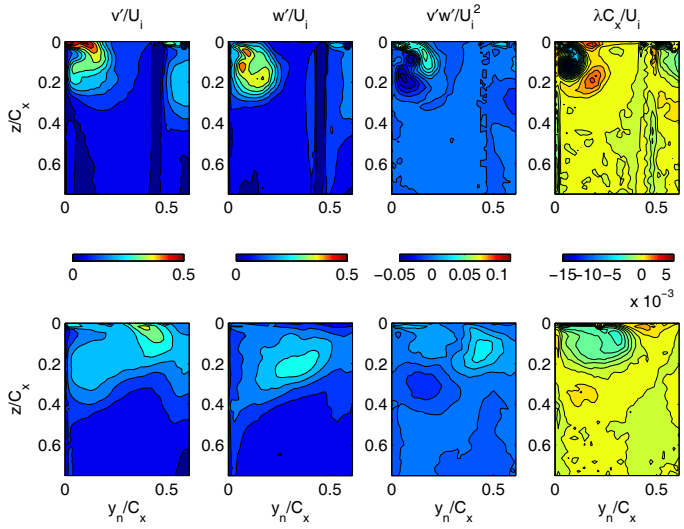

Fig. 18 Time-averaged turbulence quantities and swirl in planes 1 (top) and 2 (bottom). 3.8% tip gap, no wakes.

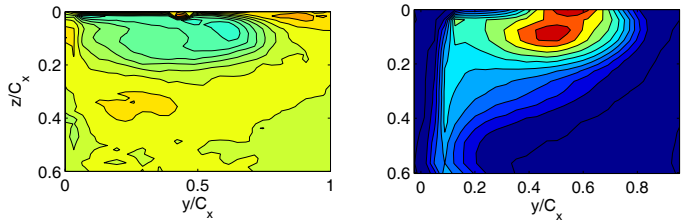

Fig. 19 Time-averaged $\lambda C_x/U_i$ (left) and ψ (right). 3.8% tip gap, no wakes.

3.8% tip gap, with wakes. In agreement with the case shown in Fig. 7, the rod wake for the case with 3.8% tip gap was present for t/T=0.5 to 0.9 in plane 1 and for t/T=1.0 to 0.4 in plane 2. The phase-averaged swirl shown in Fig. 20 exhibited little variation of the leakage vortex during the wake passing cycle in either plane. Apparently, the leakage vortex was so strong that the wakes had little effect on it. The wakes appeared to have some effect on the passage vortex, causing it to move slightly around the leakage vortex and closer to the endwall during the phases when the wake was present in plane 1, and dispersing it so that it could no longer be seen distinctly during the phases when the wake was present in plane 2. The pitchwise averaged swirl in Fig. 21 showed that the negative swirl (leakage vortex) was slightly stronger and farther from the endwall between wakes at t/T=0.6 to 0.8 in plane 2. The positive peak at z/C_x=0.2 was slightly lower at t/T=0.6 to 0.9 in plane 1, corresponding to the shift of the passage vortex closer to the endwall seen in Fig. 21. The same peak at z/C_x=0.35 in plane 2 was similarly lower at t/T=0.2, which again corresponded to the presence of the wake.

Figure 22 shows the time-averaged swirl and total pressure loss for the 3.8% tip gap case with wakes. There was very little difference from the case without wakes of Fig. 18. The swirl and loss were dominated by the strong leakage vortex, and the wake effect was apparently small in comparison.

Spatially Averaged Swirl and Loss

The pitchwise averages of the positive and negative swirl strength are shown in Fig. 23 for all cases. The results are the time-average of all data (including all phases for the cases with wakes). The pitchwise

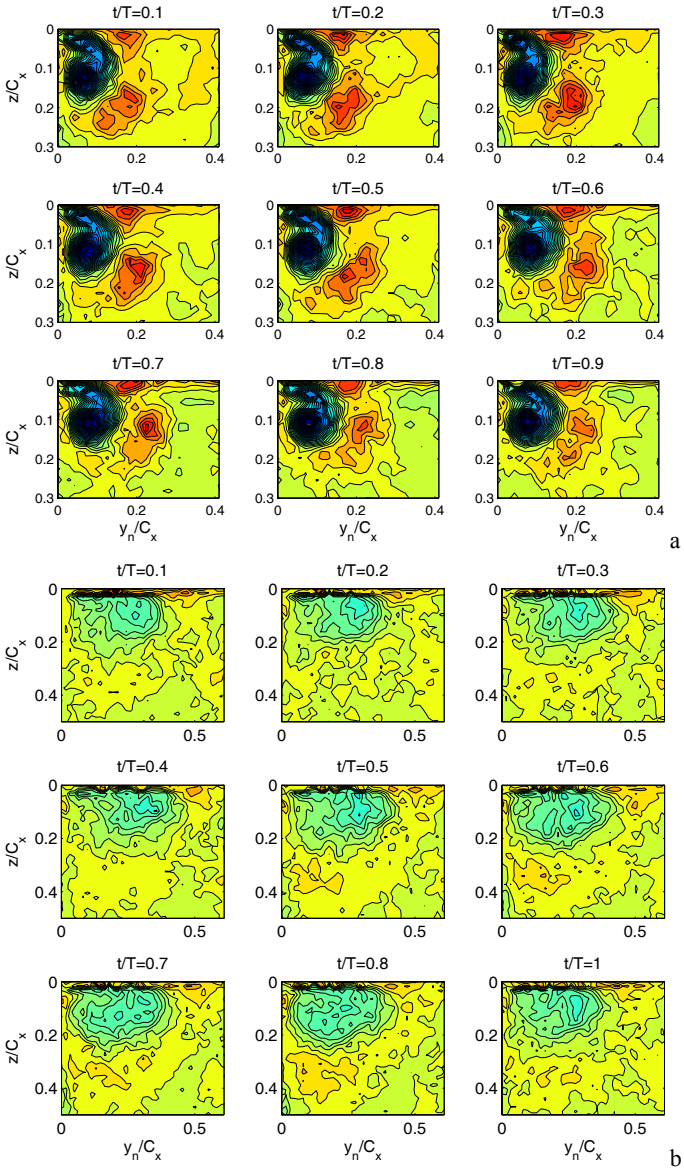

Fig. 20 Phase-averaged swirl, 3.8% tip gap: a) plane 1, b) plane 2.

averaging was done in the same way as for the phase-averaged results of Figs. 15 and 22. Comparing the open and filled symbols for each tip gap shows that the wake effect was small for the negative (clockwise, CW) swirl. For the positive (counterclockwise, CCW) swirl, the wake caused a drop in the peak associated with the passage vortex at z/C_x≈0.2 in plane 1 and z/C_x≈0.3 and in plane 2. To quantify the wake effect, the data in Fig. 23 were averaged in the spanwise direction from the endwall to z/C_x =0.6 and shown in Table 3. In the cases with a tip gap, the wakes caused the CCW swirl to decrease by roughly 15%.

The size of the tip gap had a large effect on the CW swirl, as expected since the CW swirl was caused by the tip leakage. The value of the CW swirl in Table 3 roughly doubled between the 1.5% and 3.8% tip gap cases. For the CCW swirl, the tip leakage moved the peak farther from the endwall, but the values in Table 3 show that the average magnitude of the CCW swirl did not change much as a function of tip gap size.

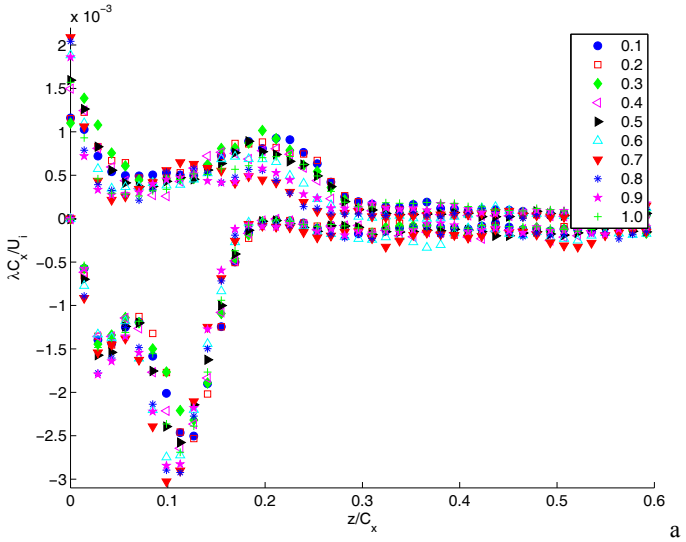

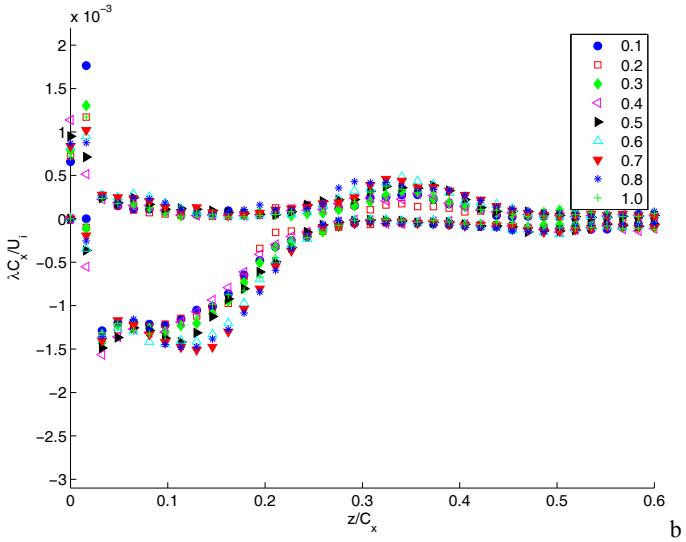

Fig. 21 Phase-averaged and pitchwise averaged swirl: a) plane 1, b) plane 2. 3.8% tip gap. Legend indicates wake passing phase from *t/T*=0.1 to 1.

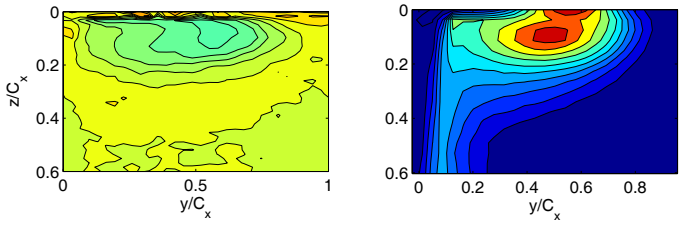

Fig. 22 Time-averaged $\lambda C_x/U_i$ (left) and ψ (right). 3.8% tip gap, with wakes.

Figure 24 shows the pitchwise averaged total pressure loss for all cases. The average of these values for z/C_x =0 to 0.6 are given in Table 3. The wakes increased ψ at all locations by an average of about 0.06. Much of this was directly attributable to the loss associated with the rod wakes themselves, but some additional loss occurred when the rod wakes interacted with the endwall and blade boundary layers. This was discussed more in Volino *et al*. [22]. The

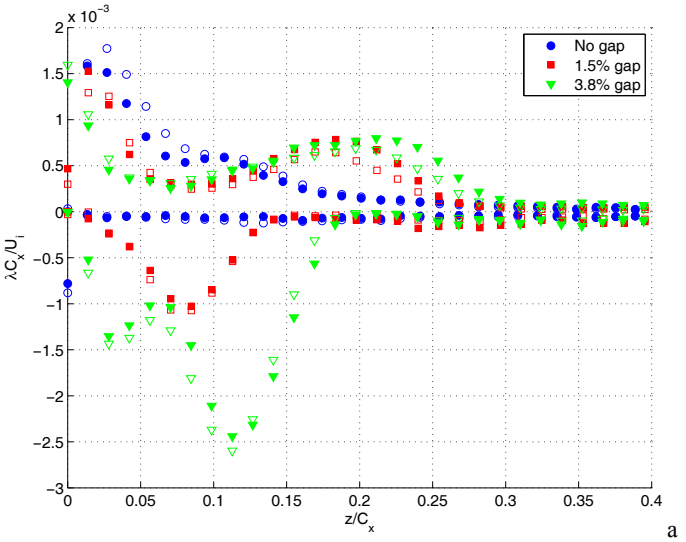

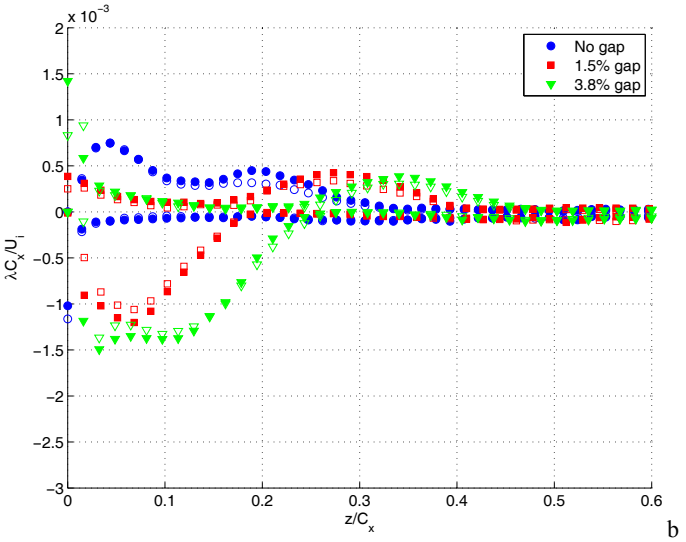

Fig. 23 Pitchwise average of time-averaged swirl, solid symbols – without wakes, open symbols – with wakes: a) plane 1, b) plane 2. Areas of time-averaged positive and negative swirl are pitchwise averaged separately.

size of the tip gap had a large effect on the loss with the average more than doubling between the no gap and 1.5% gap cases, and then increasing by another 20% between the 1.5% and 3.8% gap cases. The large near wall peak in Fig. 24 was caused by the leakage flow. Interestingly, for z/C_x>0.3, the loss was lower for the case with the larger tip gap. The leakage flow was so strong with the large tip gap that it appeared to entrain other fluid and draw it closer to the endwall, resulting in lower loss far from the wall.

CONCLUSIONS

The effects of periodic wakes generated with upstream moving rods were investigated in the endwall region of a linear cascade of high pressure turbine blades in a low speed wind tunnel. Cases were documented that included no tip gap, and tip gaps of 1.5% and 3.8% of axial chord. Total pressure loss and secondary velocity fields in the blade passages were measured. Without a tip gap, the dominant feature in the endwall boundary layer was the passage vortex. A second vortex, rotating in the same direction as the passage vortex,

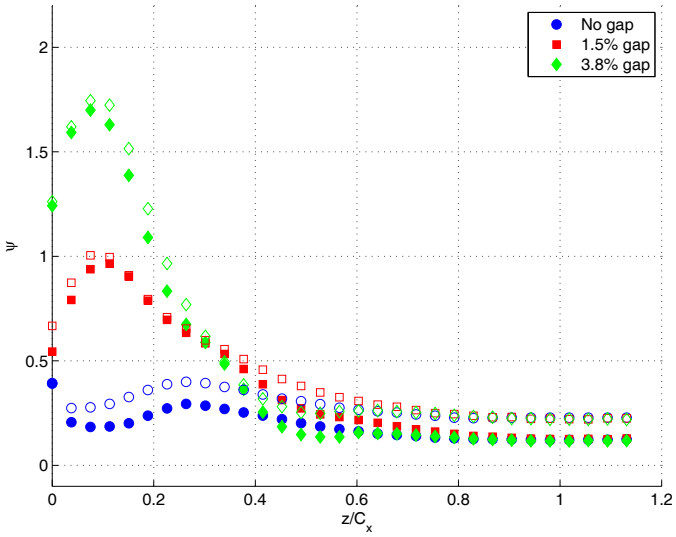

Fig. 24 Pitchwise average of total pressure loss, solid symbols – without wakes, open symbols – with wakes.

Table 3: Spatial average of time-averaged swirl and loss coefficient across one blade pitch and between 0<z/C_x<0.6.

Tip gap %	Wakes	Plane 1 $\lambda C_x/U_i \times 10^4$		Plane 2 $\lambda C_x/U_i \times 10^4$		ψ
		CW	CCW	CW	CCW	
0	No	-0.63	2.40	-0.98	2.03	0.28
0	Yes	-0.76	2.75	-0.97	1.75	0.36
1.5	No	-1.95	2.76	-2.48	1.63	0.60
1.5	Yes	-1.77	2.34	-2.21	1.23	0.63
3.8	No	-4.59	3.06	-4.12	1.77	0.72
3.8	Yes	-4.66	2.74	-3.70	1.44	0.80

was also present near the suction surface – endwall corner. This second vortex may have been induced by the suction side leg of the horseshoe vortex. When a tip gap was present, the tip leakage vortex was the strongest vortex. The passage and near-wall vortices were still present with about the same strength as in the case without a tip gap, but the leakage flow caused them to migrate away from the endwall and suction surfaces. The regions of high total pressure loss clearly corresponded to the vortices, with the highest loss associated with the tip leakage vortex. The loss in the case with 1.5% tip gap was over twice that of the case with no tip gap, and the loss increased another 20% when the gap was increased to 3.8%. Wakes caused a rise in the total pressure loss coefficient of about 0.06 in all cases, with most of the increase due directly to the upstream generated wakes and the remainder due to the interaction between the wakes and the endwall and blade boundary layers. A 0.06 increase in loss coefficient constituted about a 20%, 10%, and 8% increase in ψ for the cases with no tip gap, 1.5% tip gap and 3.8% tip gap, respectively. The wakes did not have a large influence on the endwall flow structure, but some effects were seen. Each wake caused the passage vortex to move toward the endwall. After the wake passed, the vortex returned to its undisturbed location. Near the passage exit, in the cases with a tip gap, the wakes periodically dispersed the passage vortex so that it was no longer clearly visible in phase-averaged results. The tip leakage vortex was stronger, so the wakes had less of an effect on it, particularly when the tip gap was large and the vortex was very strong.

ACKNOWLEDGMENTS

This work was sponsored by the National Aeronautics and Space Administration under cooperative agreement NNC11IA11I. The grant monitor was Dr. David Ashpis of the NASA Glenn Research Center. The second author participated in this study through the United States Naval Academy Trident Scholar program. The support of the Naval Academy Technical Support Department Shop and Fluids Laboratory was greatly appreciated.

REFERENCES

[1] Langston, L.S., 1980, "Crossflows in a Turbine Cascade Passage," *ASME J. Engineering for Power*, **102**, 866–874.

[2] Wang, H.P., Olson, S.J., Goldstein, R.J., and Eckert, E.R.G., 1997, "Flow Visualization in a Linear Turbine Cascade of High Performance Turbine Blades," *ASME J. Turbomachinery*, **119**, 1–8.

[3] Sharma, O.P. and Butler, T.L., 1987, "Predictions of Endwall Losses and Secondary Flows in Axial Turbine Cascsades," *ASME J. Turbomachinery*,. **109**, 229-236.

[4] Denton, J.D., 1993, "Loss Mechanisms in Turbomachines," *ASME J. Turbomachinery*, **115**, 621-656.

[5] Sjolander, S.A. and Amrud, K.K., 1987, "Effects of Tip Clearance on Blade Loading in a Planar Cascade of Turbine Blades," *ASME J. Turbomachinery*, **109**, 237–245.

[6] Xiao, X., Lakshminarayana, B., 2002, "Experimental Investigation of End-Wall Flow in Turbine Rotor," *J. Propulsion and Power*, **18**, 1122-1123.

[7] Harvey, N.W., 2004, "Aerothermal Implications of Shroudless and Shrouded Blades," VKI Lectures Series 2004-02, "Turbine Blade Tip Design and Tip Clearance Treatment".

[8] Booth, T.C., 1982, "Rotor-Tip Leakage Part I - Basic Methodology," *J. Engineering for Power*, **104**, 154-161.

[9] Payne, S.J., Ainsworth, R.W., Miller, R.J., Moss, R.W., and Harvey, N.W., 2003, "Unsteady loss in a high pressure turbine stage", *Int. J. Heat and Fluid Flow*, **24**, 698–708.

[10] Behr, T., 2007, "Control of Rotor Tip Leakage and Secondary Flow by Casing Air Injection in Unshrouded Axial Turbines," Doctor of Sciences Thesis, ETH Zurich.

[11] Lattime, S.B. and Steinetz, B.M., 2004, "High-Pressure-Turbine Clearance Control Systems: Current Practices and Future Directions," *AIAA J. Propulsion and Power*, **20**, 302-311.

[12] Gregory-Smith, D. G., and Cleak, J. G. E., 1992, "Secondary Flow Measurements in a Turbine Cascade With High Inlet Turbulence," *ASME J. Turbomachinery*, **114**, 173–183.

[13] MacIsaac, G.D., Sjolander, S.A., and Praisner, T.J., 2012, "Measurements of Losses and Reynolds Stresses in the Secondary Flow Downstream of a Low-Speed Linear Turbine Cascade," *ASME J. Turbomachinery*, **134**, paper 061015.

[14] Wang, J., Liu, Y., Wang, X., Du, Z., and Yang, S., 2010, "Characteristics of Tip Leakage Flow of the Turbine Blade With Cutback Squealer and Coolant Injection," ASME Paper GT2010-22566.

[15] Hodson, H.P., and Howell, R.J., 2005, "Bladerow Interactions, Transition, and High-Lift Aerofoils in Low-Pressure Turbine," *Annual Review of Fluid Mechanics*, **37**, pp. 71-98.

[16] Chaluvadi, V.S.P., Kalfas, A.I., and Hodson, H.P., 2001, "Blade Row Interaction in a High Pressure Turbine," *J. Propulsion and Power*, **17**, 892-901.

[17] Boletis, E., and Sieverding, C.H., 1991, "Experimental Study of the Three Dimensional Flow Field in a Turbine Stator Preceded by a Full Stage," *ASME J. Turbomachinery*, **113**, 1-9.

[18] Prasad, A. and Wagner, J.H., 2000, "Unsteady Effects in Turbine Tip Clearance Flows," *ASME J. Turbomachinery*, **122**, 621-627.
[19] Palafox, P., Oldfield, M.L.G., LaGraff, J.E., and Jones, T.V., 2008, "PIV Maps of Tip Leakage and Secondary Flow Fields on a Low-Speed Turbine Blade Cascade With Moving End Wall," *ASME J. Turbomachinery*, **130**, Paper 011001.
[20] Srinivasan, V. and Goldstein, R.J., 2003, "Effect of Endwall Motion on Blade Tip Heat Transfer," *ASME J. Turbomachinery*, **125**, 267–273.
[21] Krishnababu, S.K., Dawes, W.N., Hodson, H.P., Lock, G.D., Hannis, J., and Whitney, C., 2009, "Aerothermal Investigations of Tip Leakage Flow in Axial Flow Turbines – Part II: Effect of Relative Casing Motion," *ASME J. Turbomachinery*, **131**, Paper 011007.
[22] Volino, R.J., Galvin, C.D., and Ibrahim, M.B., 2013, "Effects of Periodic Unsteadiness on Secondary Flows in High Pressure Turbine Passages," ASME Paper GT2013-95881.
[23] Halila, E.E., Lenahan, D.T., and Thomas, T.T., 1982, "Energy Efficient Engine High Pressure Turbine Test Hardware Detailed Design Report," NASA CR-167955.
[24] Timko, L.P., 1984, "Energy Efficient Engine High Pressure Turbine Component Test Performance Report," NASA CR-168289.
[25] Volino, R.J., "Effects of Endwall Boundary Layer Thickness and Blade Tip Geometry on Flow Through High Pressure Turbine Passages," ASME Paper GT2014-27013.
[26] Volino, R.J., 2010, "Separated Flow Measurements on a Highly Loaded Low-Pressure Turbine Airfoil," *ASME J. Turbomachinery*, **132**, paper 011007.
[27] Hutchins, N., Hambleton, W.T., and Marusic, I., 2005 "Inclined Cross-Stream Stereo Particle Image Velocimetry Measurements in Turbulent Boundary Layers," *J. Fluid Mechanics*, **541**, 21-54.
[28] Bunker, R.S., 2006, "Axial Turbine Blade Tips: Function, Design, and Durability," *J. Propulsion and Power*, **22**, 271-285.